Int. J. Electrochem. Sci., 14 **(2019)** 6133 – 6146, doi: 10.20964/2019.07.14

International Journal of
ELECTROCHEMICAL
SCIENCE
www.electrochemsci.org

Passivation Behavior and Corrosion Resistance of 904L Austenitic Stainless Steels in Static Seawater

Dan Yang[1,2,3,5], *Yanliang Huang*[1,3,5,*], *Peng Peng*[4], *Xiangju Liu*[1,2,3,5], *Binbin Zhang*[1,3,5]

[1] CAS Key Laboratory of Marine Environmental Corrosion and Bio-fouling, Institute of Oceanology, Chinese Academy of Sciences, Qingdao 266071, China
[2] University of Chinese Academy of Sciences, Beijing 100049, China
[3] Open Studio for Marine Corrosion and Protection, Qingdao National Laboratory for Marine Science and Technology, Qingdao 266237, China
[4] CSG Power Generation Co., Ltd, Guangzhou 511400, China
[5] Center for Ocean Mega-Science, Chinese Academy of Sciences, Qingdao 266237, China
[*]E-mail: hyl@qdio.ac.cn

Received: 4 February 2019 / *Accepted:* 18 April 2019 / *Published:* 10 June 2019

The passive properties of 904L ASS in a seawater pumped storage system were studied by polarization curves, and performed by EIS and Mott–Schottky analysis. The results confirmed that the passive film formed on 904L ASS performs as n-type and p-type semiconductors at different potential ranges. The passive film that formed at 0.2 V vs. SCE has the lowest densities of donors and acceptors. The effect of temperature on the corrosion behavior of the 904L austenitic stainless steel in static seawater, which simulated the static period of seawater pumped storage systems, was determined by Tafel polarization and EIS. Based on the results of the electrochemical measurements, the corrosion rate of 904L ASS was found to increase with rising temperatures. 904L ASS has excellent corrosion resistance in static seawater. Due to its corrosion resistance, 904L ASS can be used to fabricate key structures of seawater pumped storage power systems.

Keywords: Seawater pumped storage system; 904L ASS; Passive film; Corrosion resistance; Temperature; Electrochemical measurements

1. INTRODUCTION

Pumped storage systems (PSSs) are the most mature and the most competitive technologies for large-scale energy storage [1-3]. Until now, PSSs were an important technology used to ensure the security and stability of the power grid in China. As China's coastal regions are rapidly developing, China will also need to boost its power generation capacity to meet the increased demand for electricity. Meanwhile, as concerns about environmental protection and energy security increase,

renewable energy sources that will adjust and optimise the energy mix efficiently are being considered to generate electricity. Coastal regions and islands have abundant renewable resources such as wind energy, solar energy, tide energy, wave energy, etc. Recently, the generation of electricity through the use of wind farms, solar photovoltaics, solar thermal power stations, tidal power stations and wave power stations is rapidly increasing around the world [4,5]. However, renewable resources are stochastic, and the production of renewable power is unsteady, which severely challenges the national electric grids [6]. PSSs aim to store large amounts of energy to improve the stability of the power systems, where excess electricity is stored by pumping water. By combining the use of renewable power systems, PSSs enjoy great potential and vast development prospects.

Although traditional PSSs play a vital role in the electric grid, they rely heavily on fresh water resources, which makes it more expensive and difficult to build PSSs in coastal regions and islands. Seawater pumped storage systems (SPSSs) will gradually be developed to provide the large-scale energy storage that will be required in the coming years [7]. Using the sea directly as the lower reservoir, SPSSs reduce much of the upfront costs and construction time compared with traditional PSSs. SPSSs that are either built near large power sources, such as wind power, nuclear power and solar power, or built near the coastal load centre with relatively large power demands are able to store and dispatch the electricity generated by renewable resources and guarantee the flexibility and stability of electric grids [8,9]. Until now, there was only one experimental SPSS worldwide, which was located in Japan. The Japanese SPSS is an important reference for investigating the construction and operation of similar systems. Therefore, experts and scholars across the world have performed studies on the site selection, construction, operation and maintenance of seawater pumped storage systems. The use of seawater in SPSSs introduces several issues, including the leakage of seawater, the corrosion of materials, the biofouling of marine organisms, etc. One of the key elements we are concerned with is, of course, the materials corrosion, which will occur at the location of penstocks, heat exchangers, valves and turbine blades. The operational conditions of the seawater pumped storage power plant are complex and harsh, as construction materials suffer from severe normal corrosion and local corrosion [10-12]. The temperature, operation pressure, seawater velocity and biological activities are the major factors that affect the corrosion of metal materials in marine environments [13-16]. Therefore, it is important to select corrosion-resistant materials for the key components (penstocks, pumps, hydro turbines, etc.) of SPSSs [17].

Austenitic stainless steels have been widely employed in marine engineering due to their good mechanical strength and corrosion resistance. 904L austenitic stainless steel (904L ASS) is a super austenitic stainless steel designed for more aggressive environments with long-term performance. 904L ASS contains high levels of Cr and Ni with additions of Mo and Cu and has excellent resistance to pitting corrosion, crevice corrosion, erosion corrosion and stress corrosion cracking, which is attributed to the formation of a dense passive film on the steel surface. 904L ASS can be used to fabricate the key components in alkaline and more aggressive environments compared with conventional stainless steels. Bellezze et al. [18-20] investigated the corrosion resistance of different stainless steels in a strong acid solution. The authors concluded that Cr and Mo played the most important role in the passivation and that 904L stainless steel performed much better than 316L stainless steel in the strong acid solution. Lindgren et al. [21] indicated that the ability of a material to

re-passivate was a decisive factor in attaining erosion corrosion resistance. Although 2205 DSS showed a similar re-passivation rate compared to 904L ASS, the erosion corrosion mass loss of 904L ASS was lower than 2205 DSS under a higher erosion intensity in a high temperature sulfuric acid solution.

The ability of a material to form a passive film is a key factor in determining the corrosion resistance of metals [22-25]. Until now, there have been many studies on the corrosion resistance and passivation of 904L ASS in acidic or aggressive environments [26-31]. There are few works on the corrosion resistance and passivation of 904L ASS in seawater pumped storage systems. Moreover, temperature is also an important factor that influences the corrosion resistance of stainless steel [32-35]. The seawater in SPSSs during the static period is static. This paper focuses on the analysis of the corrosion of 904L ASS during the static period, which is necessary to determine the applicability of steel in SPSSs. A study on flowing seawater conditions will be the next step. In this work, the passivation of 904L ASS in static seawater was investigated by obtaining polarization curves and performing EIS and a Mott-Schottky analysis, which included an analysis of the passive region of 904L ASS, the passivation current density and the semiconductor character of the passive film. The effect of temperature on the corrosion of 904L ASS in static seawater was measured by Tafel polarization and EIS, evaluated by the corrosion current density and the polarization resistance.

2. EXPERIMENTAL

2.1. Metal materials and immersion electrolyte

Disc-shaped 904L ASS specimens with diameters of 10 mm and thicknesses of 10 mm were used. Prior to the electrochemical measurements, electrical connection was realized via a copper wire soldered to the sample. We induced electrical contact to each coupon by soldering a copper wire (covered with rubber) to the back side of each coupon. The sample was embedded in an epoxy resin, leaving a working area of 0.785 cm^2. The exposed surfaces of all samples were subsequently abraded with 400, 600, 800 and 1000 grit silicon carbide emery papers. The samples were then rinsed with distilled water, degreased with absolute ethanol, and dried in a cool air flow.

The immersion electrolyte was seawater that was collected directly from the Huiquan Bay of Qingdao, China.

2.2. Electrochemical measurements

The electrochemical experiments were conducted in a cell filled with seawater. A traditional three-electrode system with a PS-08 multichannel potentiostat and CHI 604B electrochemical workstation were used to measure the electrochemical characteristics of the specimens. In the three-electrode system, the specimen, a saturated calomel electrode (SCE), and a platinum wire were used as the working electrode (WE), the reference electrode (RE) and the counter electrode (CE), respectively. All potentials are presented in comparison to the SCE unless otherwise noted.

In the passivation experiments, the open circuit potential (OCP) was recorded for 1 h to ensure stabilization. When the OCP was stable, a polarization curve was obtained at a potential scan rate of 0.5 mV/s, starting at a potential of -0.6 V and eventually applying a transpassive potential. The passivation current density was measured by potentiostatically applying seven potentials within the passive region, which were 0.0, 0.1, 0.2, 0.3, 0.4, 0.5 and 0.6 V. The passive films were grown as each potential was applied for 1 h to ensure that a constant stable passive film could be formed on the surface of the steel. Electrochemical impedance spectroscopy (EIS) was performed by the potentials of 0.0, 0.2, 0.4 and 0.6 V. EIS measurements were conducted with an AC amplitude of 10 mV, and the frequency was swept from 100 kHz to 10 mHz. Before the Mott-Schottky analysis, a passive film was grown at constant potentials of 0.0 , 0.2 and o.4 V vs. SCE in the solution for 1 h so that a constant stable passive film could be formed on the surface of the sample. Mott-Schottky measurements were performed by negative potential scanning from 0.8 V to -0.6 V vs. SCE with a sweep rate of 5 mV/point at a fixed frequency of 1 kHz. Each experiment was performed several times using the same conditions to ensure reproducibility.

To detect the effect of temperature on the corrosion of 904L ASS in static seawater, the OCP of the working electrode was recorded for 1 h. The polarization curves were collected starting from a potential of -250 mV below the OCP to a potential of +250 mV above the OCP in the anodic direction with a sweep rate of 10 mV/min. EIS measurements were conducted with an AC amplitude of 10 mV peak-to-peak voltage excitation, and the frequency was swept from 100 kHz to 1 mHz. The measurements were performed at 0, 10, 20, 25, 30 and 40℃ to investigate the corrosion of 904L ASS. The impedance data were interpreted by using Zsimpwin software and equivalent circuits. Each experiment was repeated several times using the same conditions to ensure reproducibility.

3. RESULTS AND DISCUSSION

3.1. Polarization measurements of the passivation performance

A polarization curve of 904L ASS was obtained at 25℃. Figure 1 shows the polarization curve of the 904L ASS in static seawater. As shown in Figure 1, a wide passive region ranging from approximately -0.1 to 0.9 V was observed, and the curve did not have an obvious active-passive transition nor an active current peak. The passivation of 904L ASS in static seawater is spontaneous. When the potential exceeded 1.1 V, the 904L ASS was in the transpassive region of the polarization curve, which was accompanied by a sharp increase in the current density. The transpassive potential was defined as the potential where the current density reached 100 $\mu A \cdot cm^{-2}$ [36]. According to previous literature [37-40], passivation occurs by dissolution-deposition. A higher potential disturbs the equilibrium between the dissolution and deposition of alloys, accelerating the dissolution rate of the passive film in seawater. For 904L ASS, transpassivation can be described as the oxidative dissolution of the chromic oxide layer [41].

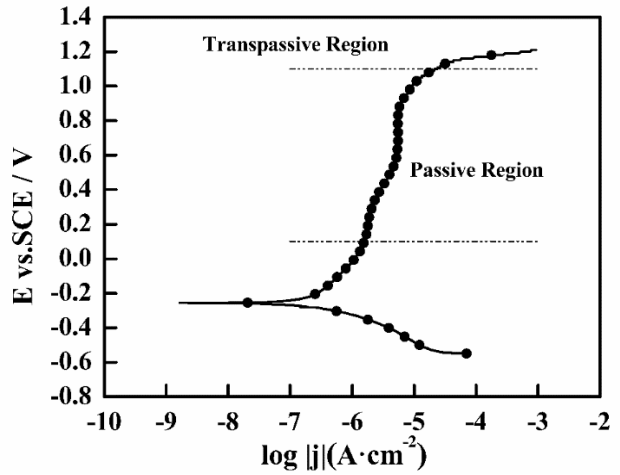

Figure 1. Polarization curve of 904L ASS in static seawater

The different potentials of 0.0, 0.1, 0.2, 0.3, 0.4, 0.5 and 0.6 V were applied to form passive films, and the evolution of the current density was recorded. Figure 2 shows the evolution of the current density during the growth of the passive films, and Figure 3 shows the steady-state passive current density (j_{ss}) plotted versus the applied potential. For the applied potentials of 0.0, 0.1, 0.2, 0.3, 0.4 and 0.5 V, the current density decreased with growth time until a constant current was established. Under these conditions, the rate of formation of the passive film must be equal to the rate of dissolution of the passive film. The curve shapes are smooth, which indicates that a stable and constant passive film forms on the surface of the 904L ASS. As the potential increased, j_{ss} increased, and the lowest j_{ss} was measured at an applied potential of 0.2 V. Spontaneously formed 904L stainless steel passive films are less stable at higher potentials. The higher the potential is, the thinner the generated passive film. Moreover, the current density abruptly increases at an applied potential of 0.6 V, which is associated with the destruction of the passive film and the dissolution of the metal [42,43].

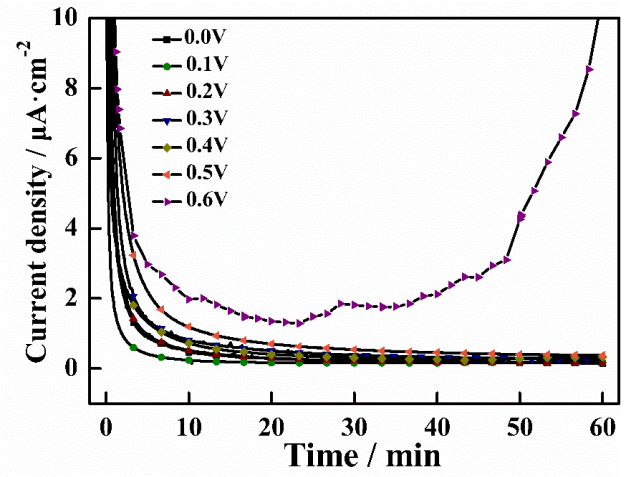

Figure 2. Current density curves of 904L ASS in static seawater measured during the 1 h growth of the passive films at different applied potentials

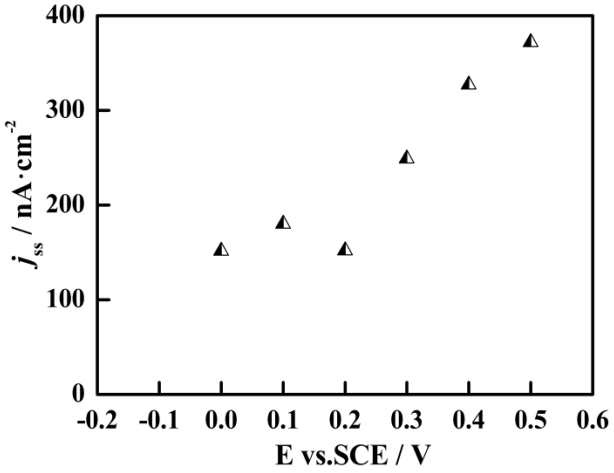

Figure 3. Steady-state passive current density of 904L ASS in static seawater obtained after the 1-h growth of the passive films at different applied potentials

3.2. EIS measurements of the corrosion resistance ofpassive film

To get a complete view of the stainless steel properties, the electrochemical impedances of the passive film were measured at selected potentials of 0.0, 0.2, 0.4 and 0.6 V. Figure 4(a) presents the Nyquist plots of the passive films formed on 904L stainless steel at different applied potentials in static seawater. As shown in Figure 4(a), there are no obvious differences in the shape of the curves obtained at the different applied potentials; only the radiuses of the capacitive arcs are different, suggesting the analogous electrochemical behaviour for all the samples. The radius of the capacitive arc at 0.2 V is the largest, and the radiuses of the capacitive arcs become smaller as the applied potentials increase, indicating weaker passivation.

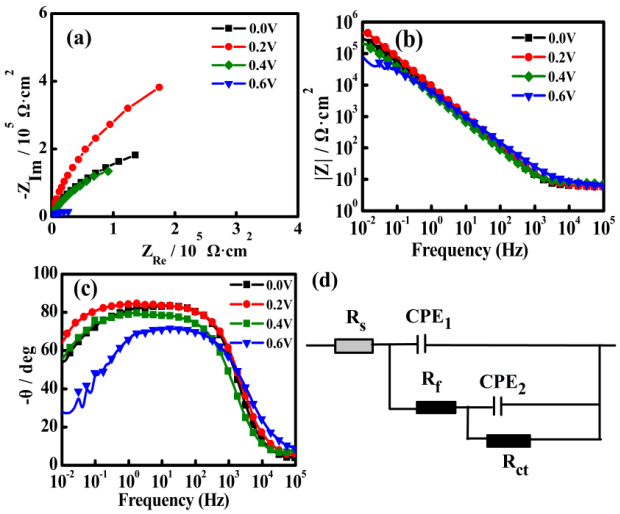

Figure 4. EIS results of 904L ASS with the 1 h growth of the passive films at different applied potentials in static seawater (a) Nyquist plots; (b) and (c) Bode plots; (d) Equivalent circuit

Figures 4(b) and (c) show the Bode plots of the passive films formed on 904L stainless steel at different applied potentials in static seawater. Many different equivalent circuit models can be used to

interpret the impedance spectra of stainless steel in alkaline solutions. The equivalent circuit shown in Figure 4(d) is employed to fit the EIS experimental results and was shown to fit the results the best [44,45]. Constant phase elements (CPE) are widely used for modelling the frequency dispersion behaviour of heterogeneous interfaces. This model assumes that the passive film is a defective layer rather than a homogeneous layer [46,47]. The equivalent circuit consists of the solution resistance (R_s) connected in series with R_f [CPE_1 (R_{ct} CPE_2)]. CPE_1 represents the capacitance of the passive film, which was connected in parallel with a resistance R_f, due to the ionic pathways through the oxide film. CPE_2 represents the double layer capacitance, which was connected in parallel with a resistance R_{ct}, representing the charge transfer resistance of the polarization process [48,49].

Table 1. Parameters obtained from the EIS results of 904L ASS with the 1 h growth of the passive films at different applied potentials in static seawater

Applied potential (V)	R_s ($\Omega \cdot cm^2$)	CPE_1 ($\mu F \cdot cm^{-2} s^n$)	n_1	R_f ($k\Omega \cdot cm^2$)	CPE_2 ($\mu F \cdot cm^{-2} s^n$)	n_2	R_{ct} ($k\Omega \cdot cm^2$)
0.0	6.105	23.1	0.93	95.1	7.53	0.63	723.9
0.2	6.233	19.5	0.93	1481.8	19.7	0.93	1641.4
0.4	7.404	39.1	0.88	308.1	20.7	0.90	207.2
0.6	6.985	34.9	0.81	39.9	3.62	0.80	12.6

Table 1 lists the best fitting parameters, according to the circuit presented in Figure 4(d). As presented in Table 1, R_f decreased as the applied potential increased, indicating that the protective abilities of the passive film are becoming weaker. R_{ct} is very high at an applied potential of 0.2 V, suggesting that the transfer process is difficult in the denser passive film. This is probably due to the stability of the chromium oxides. The polarization resistance (R_p) is commonly used as a metric of the corrosion resistance of the metal, and $R_p = R_f + R_{ct}$. The higher the R_p value is, the higher the corrosion resistance [50]. Thus, after calculation, R_p at an applied potential of 0.2 V is higher than that obtained at other applied potentials, which further confirms that the most stable passive film formed on the 904L ASS at an applied potential of 0.2 V.

3.3. Mott-Schottky analysis of film passivation

Mott–Schottky analysis was employed to determine the semiconductor type and dopant density of the passive film. The equations for Mott–Schottky analysis are as follows [51,52]:

$$\frac{1}{C_{sc}^2} = \frac{2}{\varepsilon\varepsilon_0 e N_D}\left(E - E_{Fb} - \frac{kT}{e}\right) \quad \text{for n-type semiconductors} \qquad (1)$$

$$\frac{1}{C_{sc}^2} = -\frac{2}{\varepsilon\varepsilon_0 e N_A}\left(E - E_{Fb} - \frac{kT}{e}\right) \quad \text{for p-type semiconductors} \qquad (2)$$

where ε is the permittivity of the passive film (ε=12 [43,53,54], typically), ε_0 is the permittivity of the vacuum (8.854×10^{-14} F/cm), e is the electron charge (1.6×10^{-19} C), N_D is the donor density, N_A is the acceptor density, E is the applied potential, E_{Fb} is the flatband potential, k is the Boltzmann

constant (1.38×10^{-23} J/K), and T is the absolute temperature. C is the interfacial capacitance obtained from Equation (3):

$$C = -\frac{1}{\omega Z_{Im}} \quad (3)$$

where Z_{Im} is the imaginary component of the impedance and $\omega = 2\pi f$ is the angular frequency. Assuming that the other series capacitances, e.g., the double layer capacitance and the surface state capacitance, can be neglected, the measured C is equal to the space charge capacitance, C_{sc} [42,55-57]. According to Equations (1) and (2), the plot of C_{sc}^{-2} versus E should be a straight line with a slope that is proportional to the doping concentration.

Generally, the passive film formed on stainless steel is mainly composed of an outer layer of Fe hydroxides/oxyhydroxides and an inner layer of Fe-Cr oxides [52,58]. Figure 5 shows the Mott-Schottky plots for the passive film formed on 904L ASS after immersion in static seawater for 1 h at different applied potentials. The passive film of 904L ASS in static seawater has a p-n heterojunction. For applied potentials from -0.4 to 0 V, a Mott-Schottky curve that has a straight region with a positive slope is representative of an n-type semiconductor, which reflects the semiconductivity of the outer layer where the dominant defects are oxygen vacancies and/or cation interstitials. For applied potentials greater than 0.0 V, a Mott-Schottky curve that has a straight region with a negative slope is indicative of a p-type semiconductor, which reflects the semiconductivity of the inner layer where the predominant acceptor species are cation vacancies. In particular, for applied potentials from 0.2 to 0.4 V, a Mott-Schottky curve that has a straight region with a small slope can be explained by the existence of another donor level, which might be related to the presence of molybdenum. Molybdenum ionic species might form at the passive film/electrolyte interface. In 904L ASS, molybdenum might not be a direct phase-forming element that affects the structure of the passive film.

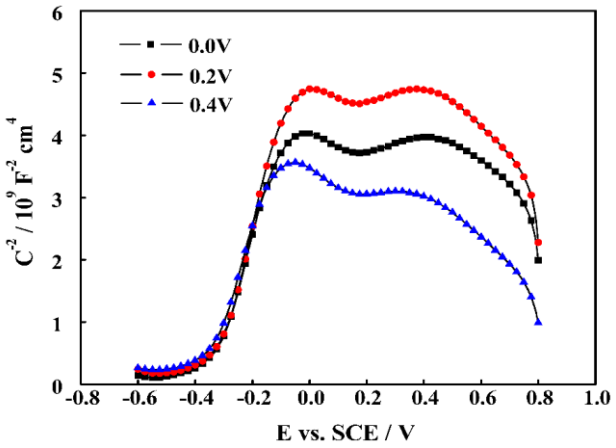

Figure 5. Mott-Schottky plots of C^{-2} as a function of potential for the passive films formed on 904L ASS after immersion in static seawater for 1 h at different applied potentials

The doping density, N, can be determined from the slopes of the Mott-Schottky curves, according to the following equation [51,52]:

$$N = \frac{2}{\varepsilon\varepsilon_0 e\sigma} \quad (4)$$

where ε is the permittivity of the passive film, ε_0 is the permittivity of the vacuum (8.854×10^{-14} F/cm), e is the electron charge (1.6×10^{-19} C), and σ is the slope of each straight line in the Mott-Schottky plots. The donor density (N_D) and acceptor density (N_A) for the n-type and p-type semiconductors are presented in Table 2. The results show that the values of N_D and N_A are in the range of 10^{20}-10^{21} cm^{-3}, which agrees with the reported values for stainless steel [58]. The results show that the values of N_D and N_A are lowest at an applied potential of 0.2 V. As was previously discussed, at an applied potential of 0.2 V, the passive film is highly ordered and the conductivities of the ferrite and chromium oxides in the passive film are the highest, which will enhance the ability of the passive film to protect the stainless steel.

Table 2. Donor density (N_D) and acceptor density (N_A) of the passive films formed on 904L ASS after immersion in static seawater for 1 h at different applied potentials

Applied potential (V)	0.0	0.2	0.4
N_D (cm^{-3})	6.74×10^{20}	5.79×10^{20}	7.32×10^{20}
N_A (cm^{-3})	3.32×10^{21}	2.71×10^{21}	2.85×10^{21}

3.4. The effect of temperature on the corrosion behavior of 904L ASS

Figure 6 shows the OCP results of 904L ASS in static seawater at different temperatures after immersion for 1 h. The OCP shifted to increasingly positive values with an increase in the immersion time, suggesting that the passive film formed on the steel surface, as expected. This is attributed to the thickening of the metal oxides film that occurs as a result of the interaction between 904L ASS and the seawater. The OCP of the specimen was stable after immersion for 1 h. The steady-state OCP values of 904L ASS at 0, 10, 20, 25, 30, and 40℃ were -97.4, -153, -181, -189, -205, and -235 mV, respectively. The OCP shifted to increasingly negative values as the temperature increased, indicating that the severity of the corrosion became greater. A higher temperature promotes the formation of the passive film, and meanwhile, it improves the absorption activity of aggressive ions on the steel surface and accelerates the dissolution of the passive film [59]. The OCP will shift to increasingly positivevalues if the formation process of the passive film is dominant. Otherwise, the OCP will decrease as the temperature increases. In this work, the harmful effect of chloride ions should make the passive film dissolve more easily [60,61], leading to the negative shift of the OCP as the temperature increases.

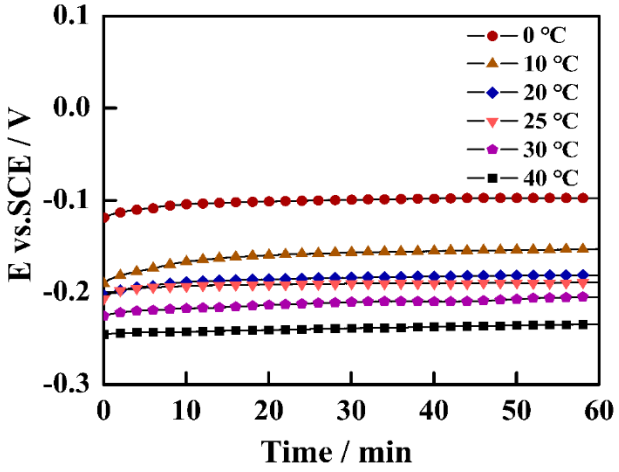

Figure 6. Evolution of the open circuit potential with immersion time for 904L ASS in static seawater at various temperatures

Figure 7 shows the polarization curves of 904L ASS in static seawater at different temperatures. Temperature simultaneously affects the anodic and cathodic reactions, resulting in the variation of the thermodynamic and kinetic parameters. The corrosion potentials and the corrosion current densities of 904L ASS in static seawater at different temperatures obtained by standard Tafel extrapolation are listed in Table 3. As shown in Table 3, E_{corr} shifted to a negative value with an increase in the temperature. The anodic dissolution of the passive film is promoted by increasing temperatures, which results in a decrease in E_{corr}. The E_{corr} values were lower than the OCP values at all temperatures, suggesting that the passive film dissolves during the potential scanning. A protective passive film is formed on the steel surface during the initial 1-h immersion.

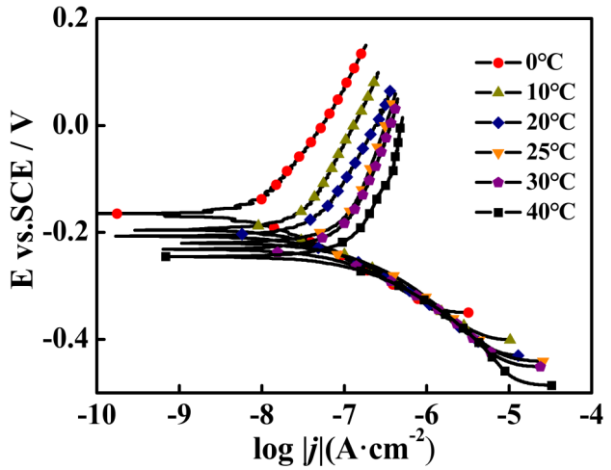

Figure 7. The polarization curves of 904L ASS in static seawater at various temperatures

The potentials of the oxide films are detected by the OCP measurement. However, the pre-existing passive film is partially removed between -0.5 V and E_{corr} in the polarization measurements. The influence of temperature on the cathodic process is not noticeable, as shown in Figure 7. In the seawater, the oxygen reduction reaction is the dominant cathodic reaction. With an increase in the temperature, the mass transfer rate of oxygen increases while the dissolved oxygen concentration in the

seawater decreases [62]. The rate of the oxygen reduction reaction is simultaneously dominated by the two processes.

Table 3. Corrosion potentials and corrosion current densities of 904L ASS in static seawater at different temperatures

Temperature (°C)	0	10	20	25	30	40
E_{corr} (mV)	-166	-194	-208	-219	-229	-246
j_{corr} (μA·cm^{-2})	0.010	0.029	0.042	0.097	0.121	0.176

Figures 8(a) and (b) show the Nyquist and Bode plots of 904L ASS in static seawater at various temperatures. The corrosion rate of 904L ASS was determined by the corrosion current density and polarization resistance. The shapes of the Nyquist and Bode plots are almost the same, while the radius of the capacitive arc decreases with an increase in the temperature. The equivalent circuit used to fit the EIS experimental data of 904L ASS at various temperatures is shown in Figure 8(c). As in the former data processing mode, the best fitting parameters obtained from the EIS results of 904L ASS in static seawater at various temperatures are presented in Table 4. As presented in Table 4, R_f decreased with an increase in the applied potential, indicating that the protective properties of the passive film were weaker. The R_f values are small at large applied potentials, indicating that the self-forming passive films that formed after immersion for 1 h in static seawater are thin and less protective. The value of R_{ct} gradually decreases with an increase in the temperature, indicating that it is less difficult for metal ions to diffuse to the corrosion layer interface.

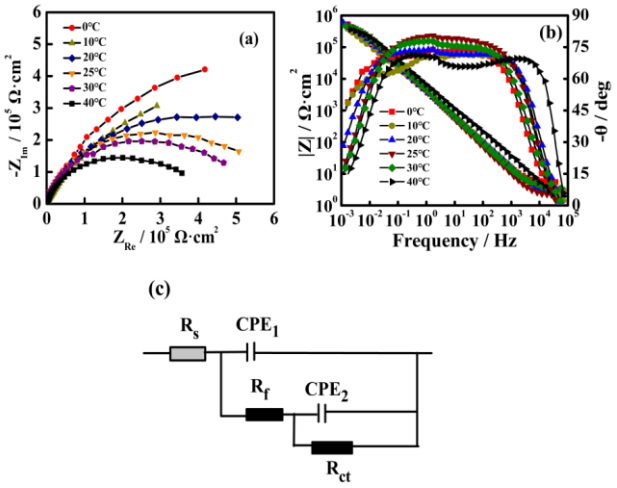

Figure 8. Electrochemical results of the (a) Nyquist plots; (b) Bode plots; and (c) Equivalent circuit of 904L ASS in static seawater at various temperatures

Thus, the corrosion of 904L ASS at 0-40°C is still controlled by diffusion mechanics [63]. The polarization resistance (R_p) is commonly used as a metric of the corrosion resistance of metals, and $R_p = R_f + R_{ct}$. It is reported that the higher the R_p value is, the higher the corrosion resistance value. The corrosion rate of 904L ASS in static seawater at various temperatures was jointly determined by the

corrosion current and the polarization resistance. The corrosion current density of 904L ASS increases as the temperature increases. Inversely, the polarization resistance of 904L ASS decreases as the temperature increases, indicating that the corrosion resistance of 904L ASS decreases with an increase in the temperature.

Table 4. Parameters obtained from the EIS results of 904L ASS in static seawater at various temperatures

Temperature (℃)	R_s ($\Omega \cdot cm^2$)	CPE_1 ($\mu F \cdot cm^{-2} s^n$)	n_1	R_f ($k\Omega \cdot cm^2$)	CPE_2 ($\mu F \cdot cm^{-2} s^n$)	n_2	R_{ct} ($k\Omega \cdot cm^2$)
0	5.201	11.8	0.97	0.058	52.4	0.69	1377.5
10	3.092	48.9	0.84	31.53	15.7	0.77	1155
20	2.519	28.6	0.89	0.47	26.5	0.75	771.6
25	2.052	36.3	0.91	0.32	10.7	0.79	567.4
30	3.891	41.3	0.86	5.52	35.4	0.90	502.8
40	1.898	13.5	0.91	0.33	34.1	0.76	431

4. CONCLUSIONS

In this work, the passivation behavior and corrosion resistance of 904L ASS in an SPSS environment under static period have been investigated by polarization curves, Tafel polarization, EIS and Mott–Schottky analysis.

(1) The potentiodynamic polarization studies demonstrated that 904L ASS displays a wide passive range in static seawater. The potentiostatic polarization tests revealed that the steady-state current densities remained very low as the passive film formed on 904L ASS for 1 h with proper applied potentials, indicating the excellent passivation behavior of 904L ASS.

(2) Based on the Mott–Schottky analysis, the passive film that formed in static seawater at different potentials values behaved as n-type and p-type semiconductor within different potential ranges. The N_D and N_A values were in the range of 10^{20}-10^{21} cm^{-3}, and the doping densities values were the lowest at an applied potential of 0.2 V.

(3) The corrosion rate of 904L ASS was determined by the electrochemical measurements. As the immersion temperature was increased, the corrosion rate of 904L ASS increased. Although the corrosion behavior of 904L ASS in static seawater was sensitive to temperature, 904L ASS still has excellent corrosion resistance at all temperatures tested in static seawater. 904L ASS can be used to fabricate the key structures of seawater pumped storage power system.

ACKNOWLEDGEMENTS
This work was financially supported by the National Key R&D Program of China (No. 2017YFB0903700 and 2017YFB0903702).

References

1. S. Rehman, L. M. Al-Hadhrami and M. M. Alam, *Renewable Sustainable Energy Rev.*, 44 (2015) 586
2. M. Guittet, M. Capezzali, L. Gaudard, F. Romerio, F. Vuille and F. Avellan, *Energy*, 111 (2016) 560
3. I. Kougias and S. Szabó, *Energy*, 140 (2017) 318
4. K. Wang, S. Chen, L. Liu, T. Zhu and Z. Gan, *Energy*, 162 (2018) 988
5. C. Schaber, P. Mazza and R. Hammerschlag, *Electr. J.*, 17 (2004) 21
6. B. Park and J. Hur, *Energy*, 164 (2018) 757
7. G. Manfrida and R. Secchi, *Energy*, 69 (2014) 470
8. E. McLean and D. Kearney, *Energy Procedia*, 46 (2014) 152
9. D. A. Katsaprakakis and D. G. Christakis, *Energy*, 66 (2014) 470
10. T. Amann, M. Waidele and A. Kailer, *Tribol. Int.*, 124 (2018) 238
11. S. Caines, F. Khan, J. Shirokoff and W. Qiu, *J. Loss Prev. Process Ind.*, 33 (2015) 39
12. H. C. Ma, Z. Y. Liu, C. W. Du, H. R. Wang, X. G. Li, D. W. Zhang and Z. Y. Cui, *Corros. Sci.*, 100 (2015) 627
13. A. López-Ortega, R. Bayón, J. L. Arana, A. Arredondo and A. Igartua, *Tribol. Int.*, 121 (2018) 341
14. W. Tian, L. Liu, F. Meng, Y. Liu, Y. Li and F. Wang, *Corros. Sci.*, 86 (2014) 81
15. M. A. Islam and Z. Farhat, *Wear*, 376-377 (2017) 533
16. F. Liu, J. Zhang, C. Sun, Z. Yu and B. Hou, *Corros. Sci.*, 83 (2014) 375
17. D. A. Katsaprakakis, D. G. Christakis, I. Stefanakis, P. Spanos and N. Stefanakis, *Energy*, 55 (2013) 619
18. T. Bellezze, G. Giuliani, G. Roventi, R. Fratesi, F. Andreatta and L. Fedrizzi, *Mater. Corros.*, 67 (2016) 831
19. T. Bellezze, G. Giuliani and G. Roventi, *Corros. Sci.*, 130 (2018) 113
20. T. Bellezze, G. Giuliani, A. Viceré and G. Roventi, *Corros. Sci.*, 130 (2018) 12
21. M. Lindgren, S. Siljander, R. Suihkonen, P. Pohjanne and J. Vuorinen, *Wear*, 364-365 (2016) 10
22. Z. H. Jin, H. H. Ge, W. W. Lin, Y. W. Zong, S. J. Liu and J. M. Shi, *Appl. Surf. Sci.*, 322 (2014) 47
23. G. Tranchida, M. Clesi, F. Di Franco, F. Di Quarto and M. Santamaria, *Electrochim. Acta*, 273 (2018) 412
24. L. A. de Oliveira, O. V. Correa, D. J. dos Santos, A. A. Z. Páez, M. C. L. de Oliveira and R. A. Antunes, *Corros. Sci.*, 139 (2018) 21
25. V. Chakarova, T. Boiadjieva-Scherzer, D. Kovacheva, H. Kronberger and M. Monev, *Corros. Sci.*, 140 (2018) 73
26. H. Luo, H. Su, C. Dong, K. Xiao and X. Li, *J. Alloys Compd.*, 686 (2016) 216
27. D. J. O. Ferreira, C. Torres, V. F. C. Lins and S. W. Park, *Mater. Corros.*, 69 (2018) 266
28. M. Lindgren, E. Huttunen-Saarivirta, H. Peltola, J. Romu, T. Sarikka, H. Hanninen and P. Pohjanne, *Corrosion*, 74 (2018) 225
29. G. B. Zou, W. Shi, S. Xiang, X. M. Ji, G. Q. Ma and R. G. Ballinger, *RSC Adv.*, 8 (2018) 2811
30. M. Lindgren, R. Suihkonen and J. Vuorinen, *Wear*, 328-329 (2015) 391
31. A. Santasalo-Aarnio, A. Lokkiluoto, J. Virtanen and M. M. Gasik, *J. Power Sources*, 306 (2016) 1
32. C. Mendibide and C. Duret-Thual, *Corros. Sci.*, 142 (2018) 56
33. X. Zhang, J. Wang, H. Fan and D. Pan, *Appl. Surf. Sci.*, 440 (2018) 755
34. E. Huttunen-Saarivirta, P. Rajala, M. Marja-aho, J. Maukonen, E. Sohlberg and L. Carpén, *Bioelectrochemistry*, 120 (2018) 27
35. Y. Han, G. Liu, D. Zou, R. Liu and G. Qiao, *Mater. Sci. Eng., A*, 565 (2013) 342
36. C. Escrivà-Cerdán, E. Blasco-Tamarit, D. M. García-García, J. García-Antón and A. Guenbour,

Corros. Sci., 56 (2012) 114
37. J. Greeley, *Electrochim. Acta*, 55 (2010) 5545
38. S. Sathyamoorthi, D. Velayutham, V. Suryanarayanan and M. Noel, *Electrochim. Acta*, 56 (2011) 7012
39. Z. Ai, J. Jiang, W. Sun, X. Jiang, B. Yu, K. Wang, Z. Zhang, D. Song, H. Ma and J. Zhang, *Cem. Concr. Compos.*, 92 (2018) 178
40. C. Albu, S. Van Damme, L. C. Abodi, A. S. Demeter, J. Deconinck and V. Topa, *Electrochim. Acta*, 67 (2012) 119
41. R. M. Fernández-Domene, E. Blasco-Tamarit, D. M. García-García and J. García-Antón, *Electrochim. Acta*, 95 (2013) 1
42. R. M. Fernández-Domene, E. Blasco-Tamarit, D. M. García-García and J. García Antón, *J. Electrochem. Soc.*, 161 (2013) C25
43. F. Gaben, B. Vuillemin and R. Oltra, *J. Electrochem. Soc.*, 151 (2004) B595
44. S. Marcelin, N. Pébère and S. Régnier, *Electrochim. Acta*, 87 (2013) 32
45. H. Luo, H. Su, C. Dong, K. Xiao and X. Li, *Constr. Build. Mater.*, 96 (2015) 502
46. F. B. Growcock and R. J. Jasinski, *J. Electrochem. Soc.*, 136 (1989) 2310
47. A. Igual Muñoz, J. García Antón, J. L. Guiñón and V. Pérez Herranz, *Corros. Sci.*, 48 (2006) 4127
48. L. Freire, M. J. Carmezim, M. G. S. Ferreira and M. F. Montemor, *Electrochim. Acta*, 56 (2011) 5280
49. G. Liu, Y. Zhang, M. Wu and R. Huang, *Constr. Build. Mater.*, 157 (2017) 357
50. E. C. Souza, S. M. Rossitti and J. M. D. A. Rollo, *Mater. Charact.*, 61 (2010) 240
51. A. D. Paola, *Electrochim. Acta*, 34 (1989) 203
52. H. Tsuchiya, S. Fujimoto, O. Chihara and T. Shibata, *Electrochim. Acta*, 47 (2002) 4357
53. N. E. Hakiki, M. D. C. Belo, A. M. P. Simoes and M. G. S. Ferreira, *J. Electrochem. Soc.*, 145 (1998) 3821
54. G. Goodlet, S. Faty, S. Cardoso, P. P. Freitas, A. M. P. Simoes, M. G. S. Ferreira and M. D. Belo, *Corros. Sci.*, 46 (2004) 1479
55. W. P. Gomes and D. Vanmaekelbergh, *Electrochim. Acta*, 41 (1996) 967
56. T. L. S. L. Wijesinghe and D. J. Blackwood, *Corros. Sci.*, 50 (2008) 23
57. A. Fattah-alhosseini, *Arab. J. Chem.*, 9 (2016) S1342
58. S. Ningshen, U. Kamachi Mudali, V. K. Mittal and H. S. Khatak, *Corros. Sci.*, 49 (2007) 481
59. M. Ben Salah, R. Sabot, P. Refait, I. Liascukiene, C. Méthivier, J. Landoulsi, L. Dhouibi and M. Jeannin, *Corros. Sci.*, 99 (2015) 320
60. C. Escrivà-Cerdán, E. Blasco-Tamarit, D. M. García-García, J. García-Antón, R. Akid and J. Walton, *Electrochim. Acta*, 111 (2013) 552
61. M. V. Cardoso, S. T. Amaral and E. M. A. Martini, *Corros. Sci.*, 50 (2008) 2429
62. M. Pour-Ghaz, O. B. Isgor and P. Ghods, *Corros. Sci.*, 51 (2009) 415
63. M. Zhu, S. Zeng, H. Zhang, J. Li and B. Cao, *Sol. Energy Mater. Sol. Cells*, 186 (2018) 200